ACS APPLIED MATERIALS & INTERFACES

Research Article

www.acsami.org

Electric Bistability Induced by Incorporating Self-Assembled Monolayers/aggregated Clusters of Azobenzene Derivatives in Pentacene-Based Thin-Film Transistors

Chiao-Wei Tseng,[†] Ding-Chi Huang,[‡] and Yu-Tai Tao*[,†,‡]

[†]Institute of Chemistry, Academia Sinica, Taipei, Taiwan

[‡]Department of Chemistry, National Tsing-Hua University, Hsin-chu, Taiwan

Supporting Information

ABSTRACT: Composite films of pentacene and a series of azobenzene derivatives are prepared and used as the active channel material in top-contact, bottom-gate field-effect transistors. The transistors exhibit high field-effect mobility as well as large *I*−*V* hysteresis as a function of the gate bias history. The azobenzene moieties, incorporated either in the form of self-assembled monolayer or discrete multilayer clusters at the dielectric surface, result in electric bistability of the pentacene-based transistor either by photoexcitation or gate biasing. The direction of threshold voltage shifts, size of hysteresis, response time, and retention characteristics all strongly depend on the substituent on the benzene ring. The results show that introducing a monolayer of azobenzene moieties results in formation of charge carrier traps responsible for slower switching between the bistable states and longer retention time. With clusters of azobenzene moieties as the trap sites, the switching is faster but the retention is shorter. Detailed film structure analyses and correlation with the transistor/memory properties of these devices are provided.

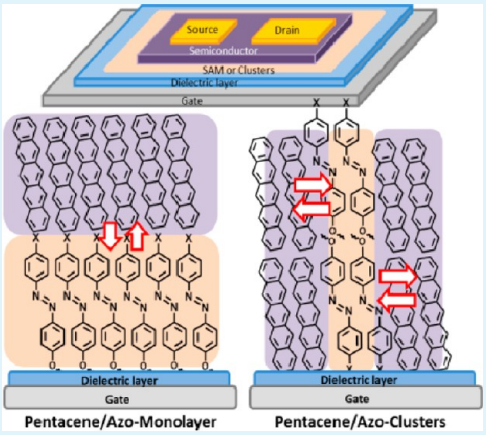

KEYWORDS: *organic field-effect transistors, electric bistability, organic memory devices*

INTRODUCTION

Memory cells are part of many electronic devices where information storage is required. With the rapid progress of organic electronics, in which organic semiconductors are used as the active channel materials, the development of organic memory cells is expected to become more and more important for the commonly cited advantages of low-cost fabrication, lightweight, and mechanical flexibility usually associated with organic materials.[1−3] Among the various types of organic memory devices,[4−7] organic field-effect transistors incorporating memory function have attracted much attention because such an approach integrates the two devices into one structure, where the switching and reading actions are performed separately. For memory devices, electric bistable states are required so that information can be stored by encoding "0" and "1" on the basis of different electric responses (for example, the conductivity) in the same material. Several mechanisms have been suggested to achieve the electric bistability in the conducting channel of a transistor.[8,9] A change of dipole moment in the dielectric layer by applying opposite gate bias has been shown to change the charge mobility and thus lead to the bistability in a conducting channel (polarization switching).[10,11] Presence of charge trapping sites in the conducting channel has also been shown to result in the electric bistability through charging/discharging of the trapping sites controlled by the gate bias (floating gate).[12,13] Metallic nanoparticles,[14−16] organic conjugated polymers,[17,18] and organic redox couples[19,20] have been used as carrier traps that collect different charge carriers and cause a threshold voltage shifts in the transfer curves of the transistor devices.

Azobenzenes are well-known to undergo photochemical isomerization of the −N═N− bond upon irradiation with light of different wavelengths.[21] The change of molecular dipole moment associated with the light-initiated isomerization (photochromism) finds numerous applications, including in organic electronics. By incorporating the photoswitchable moieties in the conducting channel, or the dielectric layer, or at their interfaces, the dopant concentration or the drift velocity of the charge carriers may be modulated upon light irradiation and results in electric bistability (polarization switching), as depicted in Scheme 1.[22−27] Other photochromic molecules such as spiropyrans have been used in a similar manner.[28,29]

On the other hand, carrier trapping has been invoked to be the origin of the switching function in systems involving azobenzene moieties under different electric bias, even though the cis−trans isomerization can also be triggered electrochemi-

Received: July 19, 2012
Accepted: September 13, 2012
Published: September 13, 2012

   dx.doi.org/10.1021/am3013906 | ACS Appl. Mater. Interfaces 2012, 4, 5483−5491

Scheme 1. Polarization Switch with Photochemical Isomerization of Azobenzene Moieties Incorporated in the Conducting Channel

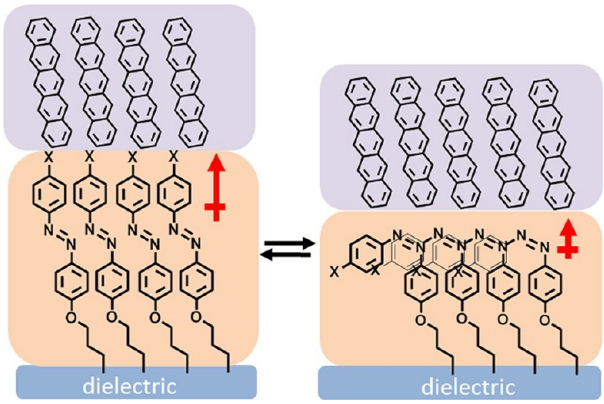

cally.[30] Thus the mechanism through which the azobenzenes affect the transistor property may not be trivial.

In this work, self-assembled monolayers(SAMs) of various substituted azobenzene moieties (through compound **1**-X, X = H, CH_3, CF_3, $C_{12}H_{25}$, structures shown in Figure 1) were

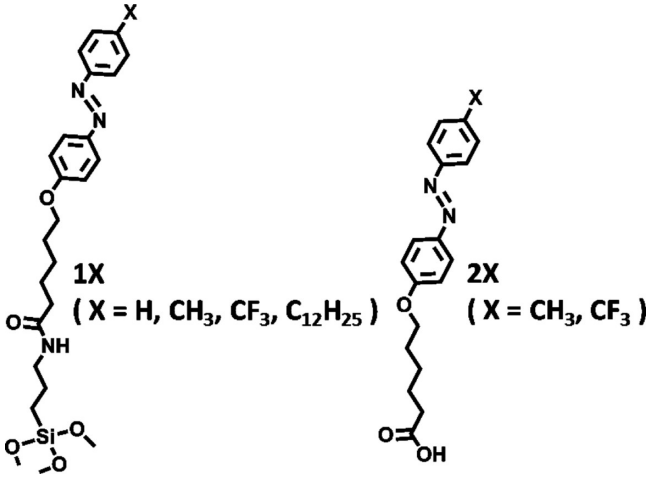

Figure 1. Structure of compounds used in the study.

prepared on a SiO_2/Si substrate surface. Pentacene films were deposited on the monolayer-covered surface and served as the channel material in a thin film transistor. Electric bistability in the pentacene film can be achieved both by photoirradiation and electric biasing. In both cases, charges are believed to be trapped at the azobenzene moieties, although through different pathways. In contrast to SAMs of azobenzene moieties, discrete clusters of multilayered azobenzene-carrying acid molecules (compound **2**-X, X= CH_3, CF_3, structure shown in scheme 1) also result in bistability in the pentacene film surrounding them. A much wider memory window and faster response associated with the systems incorporating discrete clusters versus that incorporating the monolayer are interpreted to be due to improved contact and more efficient charge transfer between conducting channels and the trapping sites. The improved contact also facilitates the dissipation of charges (discharging) at the trapping sites and leads to shorter retention time.

EXPERIMENTAL SECTION

The azobenzene-containing trimethoxysilanes (**1**) and azobenzene-containing carboxylic acids (**2**) were synthesized in the laboratory and fully characterized by ^{1}H NMR and ^{13}C NMR, mass spectrometer (see the Supporting Information).

n-Type silicon (100) substrates covered with 300 nm-thick, thermally grown oxide layer (SiO_2/Si) was cleaned by Piranha (70% H_2SO_4:30% H_2O_2) solution, thoroughly rinsed with pure water and dried by a stream of N_2. Self-assembled monolayers of **1** were prepared by immersing freshly cleaned SiO_2/Si substrates in a 1 mM THF solution of **1** for 4 h., followed by thorough rinse with pure THF. Discrete clusters of **2** were prepared by vapor deposition of **2** on cleaned SiO_2/Si substrates in a vacuum chamber. The transistor devices were prepared by depositing 60 nm pentacene film on the SAM-modified substrate (or azobenzene clusters-covered substrate) at a rate of 0.2 Å/s under a vacuum of 2×10^{-5} Torr. Source and drain electrodes were deposited through a shadow mask to achieve a top-contact, bottom-gate FET device with a channel length of 50 μm and a channel width of 500 μm.

UV-irradiation was delivered by a UV lamp (365 nm wavelength) with an intensity of 4 mW/cm^2 held at 3 cm distance from the sample under ambient condition. Attenuated total reflectance infrared spectra were recorded with a Varian 640-IR spectrometer equipped with a MCT detector at a 4 cm^{-1} resolution at room temperature.

Atomic force microscopy analyses were carried out with a Multimode Atomic Force Microscope (Digital Instruments, Nanoscope III) using tapping mode with a silicon tip. The powder X-ray diffraction measurements were carried out with a Philips X'Pert diffractometer equipped with an X'Celerator detector. The electrical characteristics of the transistor devices were measured in ambient with a HP4156 parameter analyzer.

RESULTS AND DISCUSSION

Characterization of the Surface Films. The monolayer of azobenzene-containing silane was prepared by adsorption of compound **1** onto the SiO_2/Si surface through hydrolysis, surface anchoring and dehydration process.[31] Ellipsometry and attenuated total reflectance infrared spectroscopy (ATR-IR) were used to monitor the monolayer formation process (see the Supporting Information). For example, a limiting film thickness of ~2.6 nm for **1**-CF_3 was reached after the substrate was immersed in the corresponding silane solution for 4 h, indicating the formation of monolayer (~2.8 nm for stretched length of the compound) (see Figure S1 in the Supporting Information). The ATR-IR showed the absorption peaks at 1600, 1500, and 1300 cm^{-1}, whose intensities increased with the soaking time and reached a maximum after four hours of soaking (see Figure S2 in the Supporting Information). These peaks are assigned to the C═C stretching of benzene ring, N═N and symmetric CF_3 stretching for the azobenzene moieties, respectively, indicating the presence of a monolayer.[32] Water contact angles were measured for various SAM-modified surfaces and hydrophobic surfaces (θ(H2O) > 99°) were obtained in all cases.

Sixty nanometer-thick pentacene films deposited on the monolayer-covered SiO_2 surfaces were characterized by X-ray diffraction and AFM microscopy. Polycrystalline films of pentacene were formed on all of the azobenzene monolayer surfaces, as suggested by the X-ray diffraction patterns (Figure 2) and AFM micrographs (Figure 3). A small dependence of the diffraction peak intensity on the terminal functional group was observed among the films, which might be due to different surface energy.[33] Also included in the figures are the pentacene films deposited on a monolayer of *n*-octadecyltrichlorosilane (OTS) and *n*-decyltrimethoxysilane (C_{10}), or from a 1:1

dx.doi.org/10.1021/am3013906 | ACS Appl. Mater. Interfaces 2012, 4, 5483−5491

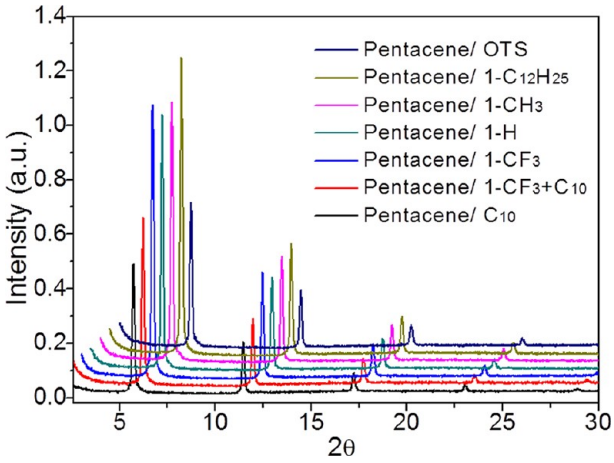

Figure 2. X-ray diffraction patterns of pentacene films deposited on various azobenzene silane- and *n*-alkane-silane monolayer-covered surfaces.

mixture of **1-CF$_3$**/C$_{10}$. It is worth noting that the diffraction peak intensity for pentacene deposited on differently substituted **1** is higher than that on the *n*-alkylsilane-modified surfaces, and the pentacene film on **1-C$_{12}$H$_{25}$** has the highest intensity. The peak intensity is in turn higher on the single component C$_{10}$-modified surface than on a surface modified by a mixed monolayer of **1-CF$_3$+C$_{10}$**. This is attributed to the molecularly rough surface formed by a mixed monolayer.[34,35]

The AFM micrographs show typical terraced grains of the pentacene layers. The grain size ranged from about 0.2 to 1 μm. The pentacene film on **1-C$_{12}$H$_{25}$** monolayer surface has larger average grains than that on the other monolayers, whereas the film on the mixed monolayer of **1-CF$_3$**/C$_{10}$ apparently has smaller grain size than those on single component SAM. This corroborates with the diffraction peak intensity results in the X-ray measurement discussed above.

Electrical Properties. Field-effect transistors were fabricated on the pentacene-azobenzene composite films in a bottom-gate, top-contact configuration by depositing gold source and drain electrodes on the films through a shadow mask. Typical *p*-type behavior was observed in that increasing current was obtained with increasingly negative gate bias after a finite threshold voltage when the gate bias was swept from +80 V to −80 V (Figure 4). Field-effect mobility values were extracted from the *I*−*V* characteristics and are listed in Table 1. The mobilities are comparable between devices prepared on different SAM-modified substrates (0.27−0.35 cm^2 V^{-1} s^{-1}), except for the film deposited on the mixed monolayer of **1-CF$_3$**/C$_{10}$, which has apparently smaller mobility than that on the single component SAM. Also the mobility is greater for the film deposited on the azobenzene SAM carrying a C$_{12}$H$_{25}$ chain. Presumably this is due to the different crystallinity of the pentacene films, as suggested by the X-ray and AFM results. The threshold voltage shifted to more positive values for devices with **1-CF$_3$** monolayer (or its mixed layer)-modified dielectric surface and shifted to more negative values for devices on **1-H** and **1-CH$_3$** monolayer-modified surfaces, compared to the typical OTS-modified reference surface. This might be due to the nature of the dielectric layer, that is, the fluorinated surface results in a positive field-effect onset voltage, whereas dielectric surfaces with electron-rich modifiers result in negative onset voltage.[24,25] Repeated scans from +80 V and −80 V at a scan rate of ∼25 V s^{-1} yield overlapping traces of I_{DS}, suggesting that no threshold voltage shift resulted from mere scanning the gate bias.

In light of the well-known UV-initiated *trans*−*cis* isomerization of azobenzene moieties, which may cause a change in the direction and magnitude of the overall dipole moment associated with an oriented monolayer at the semiconductor/dielectric interface,[36] the effect of UV-irradiation on the transfer characteristics was examined. Control experiments with pentacene-based transistor in the absence of the azobenzene SAM confirmed the photochemical stability of pentacene thin films, as indicated by the invariance of transfer characteristics with UV irradiation. This stability was also suggested in a previous work.[37] However, with UV-irradiation on the sample

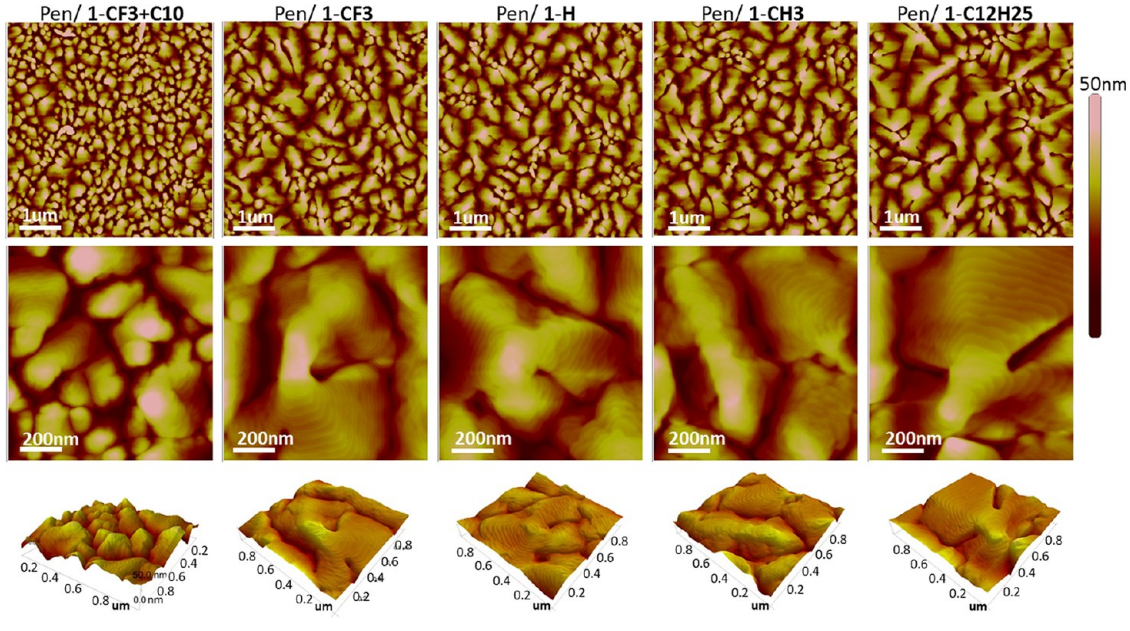

Figure 3. AFM topographic images of pentacene films deposited on various azobenzene silane monolayer-covered silicon substrates.

dx.doi.org/10.1021/am3013906 | ACS Appl. Mater. Interfaces 2012, 4, 5483−5491

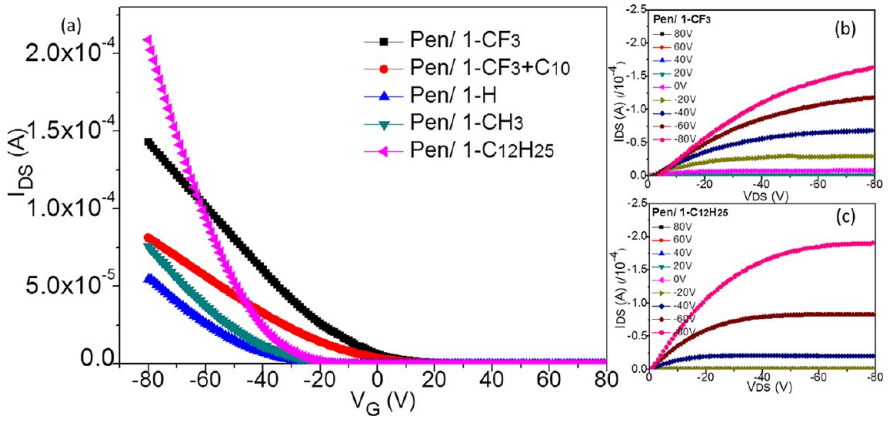

Figure 4. (a) Transfer characteristics of the devices with various SAMs-modified dielectrics. (b, c) Output characteristics of the devices with **1-CF$_3$** and **1-C$_{12}$H$_{25}$**, respectively.

Table 1. Device Characteristics As a Function of Azobenzene Silane-SAM Used

SAM	threshold voltage V_{th} (V)	mobility[a]	on−off ratio	max. V_{th} after positive gate bias (V)	max. V_{th} after negative gate bias (V)
1-CF$_3$	22.3	0.26	1×10^4	77.5	−5.2
1-CF$_3$+C$_{10}$	16.5	0.17	1×10^5	50.2	−3.4
1-H	−17.5	0.27	1×10^6	9.6	−49.5
1-CH$_3$	−17.3	0.35	1×10^7	−11.6	−56.7
1-C$_{12}$H$_{25}$	−20.3	1.04	1×10^6	−17.3	−27.1
OTS	−6.5	0.30	1×10^6	−3.3	−11.8

[a]The field-effect mobility was estimated by the plot of the square root of source to drain current $(I_{DS})^{1/2}$ versus the gate bias (V_G) from the equation in the saturation regime.

of pentacene deposited on **1-CF$_3$** SAM-modified SiO_2/Si, a small threshold voltage shift, ΔV_{th}, toward the positive direction was observed, with the magnitude of shift depending on the length of UV irradiation: a longer UV irradiation resulted in a larger shift and saturation of the shift was reached after 30 min irradiation (Figure 5a). When the irradiated device was kept in dark for various length of time, the transfer characteristics showed an opposite trend in that the threshold voltage shifted in the negative direction with time, and eventually the curve returned to the original trace (Figure 5b). In contrast, similar UV-irradiation resulted in an opposite trend of ΔV_{th} change for **1-CH$_3$**- and **1-H**-based devices. The trend is rather repeatable and reversible. Apparently the nature of the substituent (electron-donating or electron-withdrawing) has different effects on the direction of the shift.

Previous studies showed that a self-assembled monolayer carrying azobenzene moieties may not be able to undergo isomerization in a closely packed monolayer environment

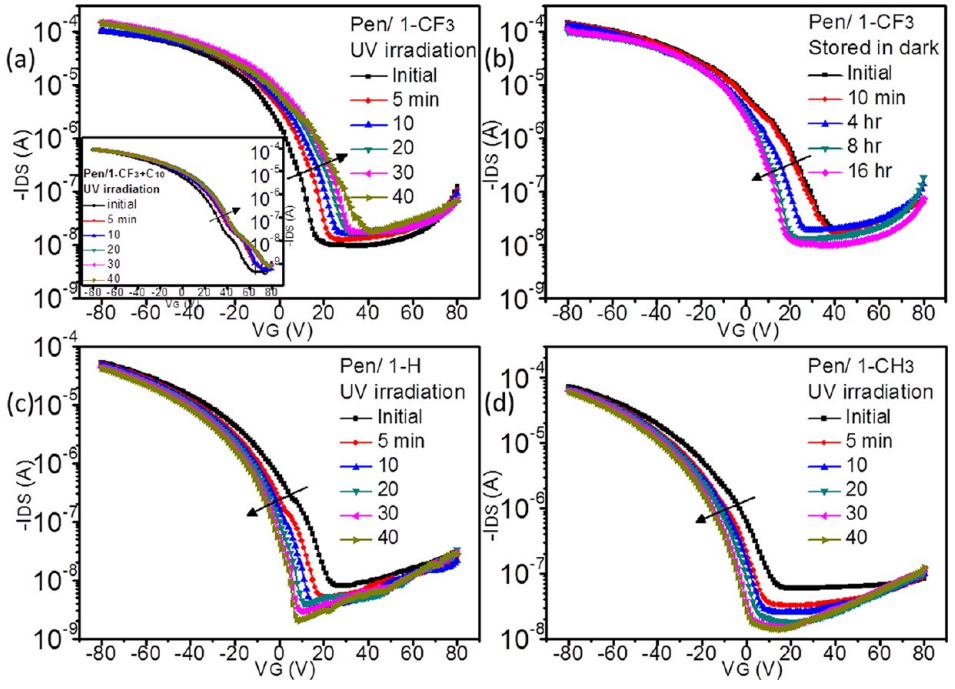

Figure 5. Transfer characteristics of devices with the monolayer of (a) **1-CF$_3$**, (c) **1-H**, and (d) **1-CH$_3$** as a function of UV irradiation (356 nm), and (b) **1-CF$_3$** device stored in dark after UV irradiation. Insert in a shows the curves for mixed monolayer of **1-CF$_3$**+C$_{10}$.

dx.doi.org/10.1021/am3013906 | ACS Appl. Mater. Interfaces 2012, 4, 5483−5491

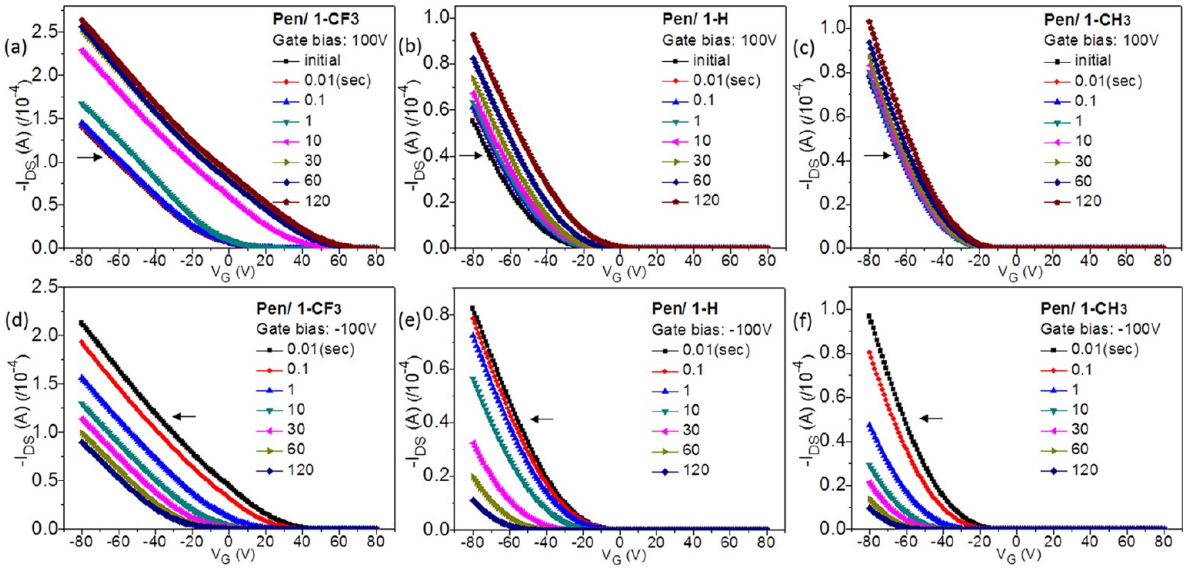

Figure 6. Transfer characteristics of devices with the monolayer of **1-CF$_3$**, **1-H**, and **1-CH$_3$** as a function of (a–c) +100 V gate pulse and (d–f) −100 V gate pulse, respectively.

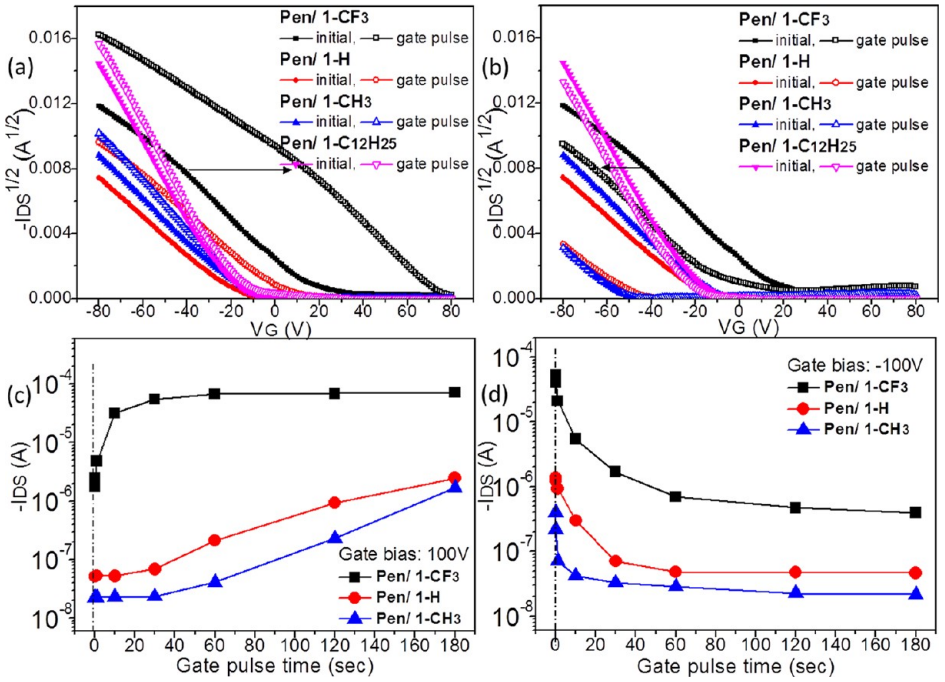

Figure 7. (a, b) Transfer characteristics of the devices after gate bias pulse of 100 V and −100 V for 60 s, respectively. (c, d) Source–drain current as a function of gate pulse time for the **1-CF$_3$**, **1-H**, and **1-CH$_3$** covered device, respectively.

because of the limited space for the trans–cis isomerization to occur.[38,39] Use of a mixed monolayer containing a shorter chain component may create additional room between the azobenzene moieties for isomerization. Thus 1:1 mixed monolayer of **1-CF$_3$** with *n*-decylsilane (C_{10}) were prepared and the pentacene film-based devices were fabricated. When gate bias was scanned under similar conditions, similar but smaller trend of shifts as for the single component **1-CF$_3$** device was observed (inset of Figure 5a). Thus the release of steric congestion by using spacers did not increase ΔV_{th}. The reduction of ΔV_{th} may only reflect the reduced density of azobenzene moieties in the system. The observation is in contrast with the model involving isomerization in the monolayer system upon irradiation. This argument will be elaborated further below.

Alternatively, when a positive gate bias pulse of +100 V was applied before the I_{DS} was measured as a function of gate bias sweep, a threshold voltage shift was also observed. In contrast to the photochemical cases above, where different directions of shift were observed for differently substituted azobenzenes, here all systems shifted in the same positive direction (Figure 6a,c,e), only to a different extent and "speed". In **1-CF$_3$** system, a greater shift (~55 V) was observed with the saturation state reached rather fast, say, in 10–30 s. For **1-CH$_3$**, the shift was smaller (~6 V) and the saturation was not reached until after 60s of initial pulse. The magnitude of the shift for the **1-H**

dx.doi.org/10.1021/am3013906 | ACS Appl. Mater. Interfaces 2012, 4, 5483–5491

system lies somewhere in between that of the other two systems (~27 V).

Furthermore, when a −100 V gate bias pulse was applied, the threshold voltage shifted in negative direction, more shift with longer pulse time (Figure 6b, d, f). In contrast, for **1-$C_{12}H_{25}$** system, only a very small shift (~3 V) was observed under the same sweeping conditions in either direction. When the ultimate shifts with the same pulse time are compared in the same plot, one sees a clear difference in the amount of shifts with substituent (Figure 7a, b). With +100 V gate pulse, the **1-CF_3** has the largest shift to the right, whereas with −100 V gate pulse, the **1-CH_3** system has the largest shift to the left. The shifts as a function of pulse time, which relates to the "response" of the switching, can also be seen in the plots of I_{DS} vs gate pulse time (Figure 7c,d). Upon an application of +100 V gate pulse, the **1-CF_3** system reached the maximum current (and thus the "ON" state) quicker, in 20 s, whereas for the **1-H** and in particular **1-CH_3** systems, the current increased slowly and did not yet reach a maximum after 180 s. At −100 V gate bias, the **1-CH_3** system reached the minimum current (and thus the "OFF" state) rapidly, in ~20 s (Figure 7c), whereas the **1-CF_3** system reached the "OFF" state slower, after >60 s (Figure 7d).

The observation of threshold shifts above, from photo irradiation or electric bias, can be rationalized as follows. We will address the effect of electric bias first. When a +100 V gate bias is applied, negative charge carriers are accumulated at the pentacene/dielectric interface. These charges can also be transferred from pentacene molecules to the azobenzene moieties. With CF_3-substituted azobenzene, the negative charges are more readily trapped and stabilized in the monolayer. More charges will be trapped with a longer pulse time. These negative charges can shield the gate bias so that the hole carriers are induced (and channel turned on) at less negative gate bias when gate is swept from +80 V to −80 V, causing the threshold voltage to shift in the positive direction. With **1-H** and more so with **1-CH_3**, where negative charges can not be well stabilized, the charges are trapped slower and less efficiently and the charging of monolayer takes longer time (Figure 7a). The threshold voltage shifts to a smaller extent (Figure 6e). When a −100 V gate bias pulse is applied, hole carriers are accumulated at the interface and some will be trapped in the azobenzene monolayer. Hole carriers are more readily transferred to the SAM of **1-CH_3**, which has an electron-donating CH_3 group to stabilize the positive charge. This positively charged layer will shield the gate bias and results in the threshold voltage in the negative direction when the transfer curve is measured. The "OFF" current is reached quicker (shorter pulse time, ~10 s) to its minimum value (Figure 7d) and a larger ΔV_{th} for the transfer curves is observed. For **1-CF_3** system, transfer of positive charges to the azobenzene moieties is less facile so that a smaller ΔV_{th} is observed and the "OFF" current is reached slower (~60 s). For **1-$C_{12}H_{25}$** system, where a long hydrocarbon chain matrix is separating the pentacene layer and the azobenzene moieties, the transfer of charges, positive or negative, from pentacenes to the azobenzene moieties is much less facile than in the case of the shorter chain **1-CH_3** layer. The ΔV_{th} in either direction are rather small. The magnitude of threshold voltage shift depends on the areal density of charges trapped at the interface, which can be estimated according to the eq 1[15,40]

$$\Delta V_{th} = \frac{d_i Q}{\varepsilon_i} = -\frac{Q}{C_i} \quad (1)$$

where C_i is the dielectric capacitance and ΔV_{th} is the threshold voltage shift. For **1-CF_3** monolayer which yielded a maximum shift of 55 V when a positive gate bias pulse is applied, the total density of electrons trapped is calculated to be 3.9×10^{12} cm^{-2}, based on C_i = 11.5 $nFcm^{-2}$. Compared to the density of molecules in the monolayer (~ $4.0 \times 10^{14}/cm^2$, based on the cross-section area of 25.2 $Å^2$ occupied by each **1-CF_3** molecule in a closely packed monolayer), about one electron is trapped in every 100 molecules. The other systems trap much smaller density of charges.

In the case of photo irradiation, the azobenzene chromophore is pumped to the excited state, making it more susceptible to oxidation as well as reduction.[41] In the case of **1-CF_3**, electron transfer from pentacene may occur to give the negatively charged state. Longer exposure time will increase the negative charge build-up in the monolayer, thus providing an additive contribution to the gate electric field that induces positive charge carriers in the pentacene accumulation layer, resulting in an earlier turn-on of the device (or a threshold voltage shift in the "positive" direction), when the transfer curve is measured. When kept in the dark, the negatively charge **1-CF_3** can lose the charges with time and threshold voltage shifts in negative direction. For **1-CH_3** (as well as **1-H**), the excited state of azobenzene is a better reductant and lose its electron to pentacene nearby to form positively charged state, which shields the gate electric field, thus resulting in the threshold voltage shifts in the "negative" direction. The process is illustrated with the energy alignment diagram in Figure 8. It is

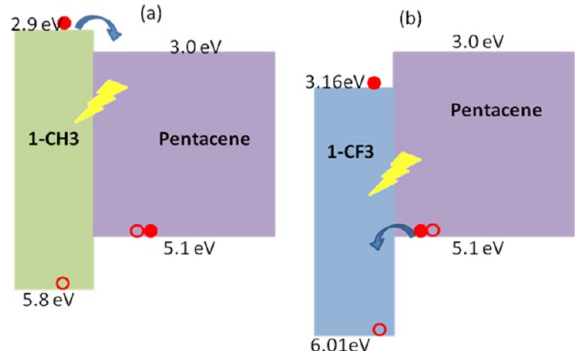

Figure 8. Energy alignment diagram showing the light-induced charge transfer between the azobenzene moieties and the pentacene: (a) generation of positively charged **1-CH_3**; and (b) generation of negatively charged **1-CF_3**.

noted that pentacene can also be excited by UV-irradiation. But the electron transfer from the HOMO of **1-CH_3** to the HOMO of excited pentacene is an uphill process in terms of energy. Photoinduced charge transfer between semiconductor molecules and gate dielectrics has been suggested to occur in several transistor systems, resulting in threshold voltage shifts.[42,43] The notion that photoinduced trans−cis isomerization did not occur in the system under consideration is further reinforced by the fact that isomerization of azobenzene in the oriented **1-CF_3** monolayer is expected to decrease the dipole moment (from −5.06 D for the trans form to −4.13 D for the cis form). This would inevitably lead to a threshold voltage shift in the negative

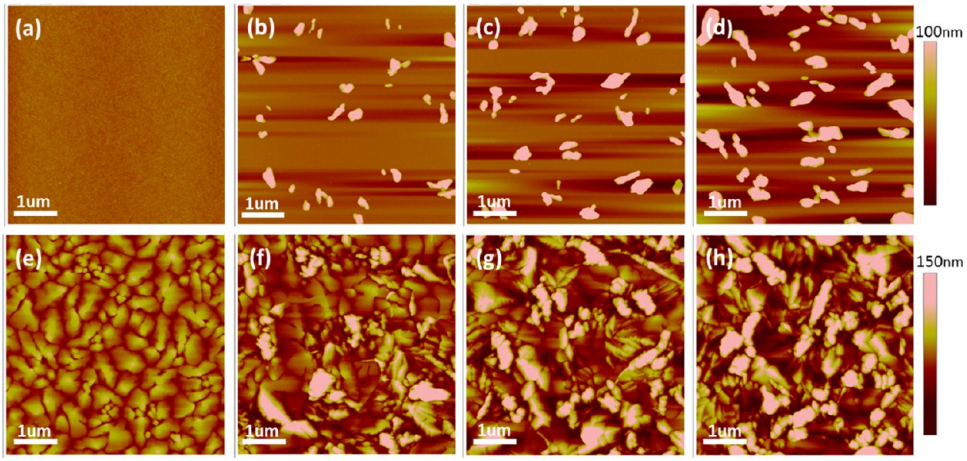

Figure 9. AFM images of silicon substrate with (a) **1-CH$_3$** monolayer, and (b–d) **2-CH$_3$** clusters prepared by thermal evaporation to a nominal thickness of 2.5, 5.0, and 10 nm, respectively; (e–h) 60 pentacene films deposited on corresponding substrate surface in (a–d).

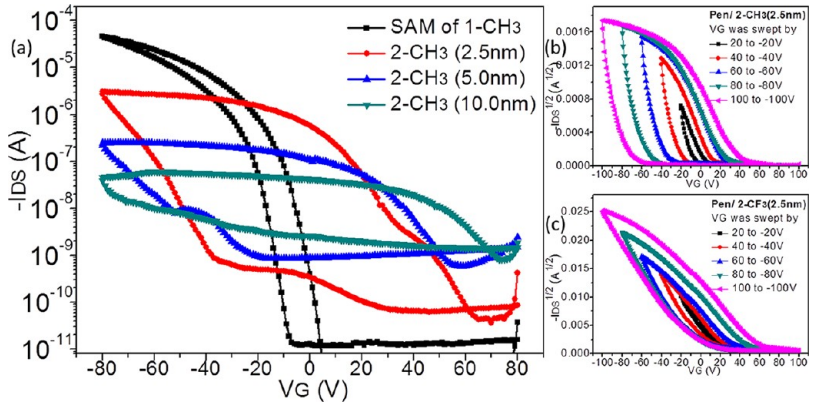

Figure 10. (a) Transfer characteristics with bidirection scan of gate voltage for the devices of **1-CH$_3$** and **2-CH$_3$** with different nominal thicknesses; (b, c) transfer characteristics as a function of scan ranges of the gate bias for the **2-CH$_3$** and **2-CF$_3$** device with a nominal thickness of 2.5 nm, respectively.

direction, in contradiction to what was observed in our experiment.

With the gate bias cycling between +80 V and −80 V, an *I*–*V* hysteresis was observed, signaling the "ON" and "OFF" states occurring when the gate bias was swept in different directions. The threshold voltage difference (or the "memory window") depends on the amount of charges trapped at the interface, as well as how fast the charges are trapped during a bias sweep. In an earlier work we demonstrated that the rate of charging the trapping sites depends on the proximity of the charge conduction path to the trapping sites.[17] With the trapping sites (the azo groups) residing within the monolayer at the dielectric surface, the charge transfer can occur only from the few nearest molecular layers of pentacene on top of the SAM, through the barrier created by the SAM's substituent or molecular fragments. For example, with **1-C$_{12}$H$_{25}$**, the charge transfer is suppressed because of the long insulating alkyl chains. To bring the accumulation channel and the trapping sites closer to each other, one can incorporate discrete clusters with pentacene situated close to the azobenzene moieties. Discrete clusters of azobenzene moieties were prepared by thermal deposition of compound **2** on a cleaned silicon substrate surface. Figure 9 shows the AFM micrographs of **2-CH$_3$** deposited on the substrate up to a nominal thickness of 2.5, 5, and 10 nm, respectively. Randomly distributed and well-separated clusters of 50–200 nm in dimension and 50–100 nm in height were obtained. These are expected to be multilayers of dimers of **2** through hydrogen bonded carboxyl groups. Also included in the figure is the AFM image of a monolayer of **1-CH$_3$**, exhibiting a featureless and smooth surface in contrast. An effective thickness of 2.5 nm of **2-CH$_3$** is equivalent to a monolayer of **1-CH$_3$** and it is assumed that 2.5 nm clusters contain similar amount of azobenzene moieties as in a SAM of **1-CH$_3$**. X-ray diffraction measurement of these films show that the thicker the film of **2-CH$_3$**, the lower the crystallinity of pentacene film deposited on it.

When the gate bias was cycled between +80 V and −80 V, a clear hysteresis was observed as a function of the thickness of **2-CH$_3$** films deposited on the surface and the more azobenzene moieties are present at the interface, the greater the hysteresis (and the memory window) (Figure 10a). Presumably, the more charges can be trapped at the interface, the greater the shielding effect and the larger the threshold voltage shifts. It can also be seen that the ON/OFF ratio decreases with increasing amount of **2-CH$_3$** at the interface. This may be attributed to 1) decreasing crystallinity of pentacene films on thicker azobenzene layers, and thus lower mobility in the ON state; and 2) the thicker charge trapping layer increases the residual charges trapped there and increases the OFF current and thus decreases the ON/OFF ratio. It is also worth noting that in

dx.doi.org/10.1021/am3013906 | ACS Appl. Mater. Interfaces 2012, 4, 5483–5491

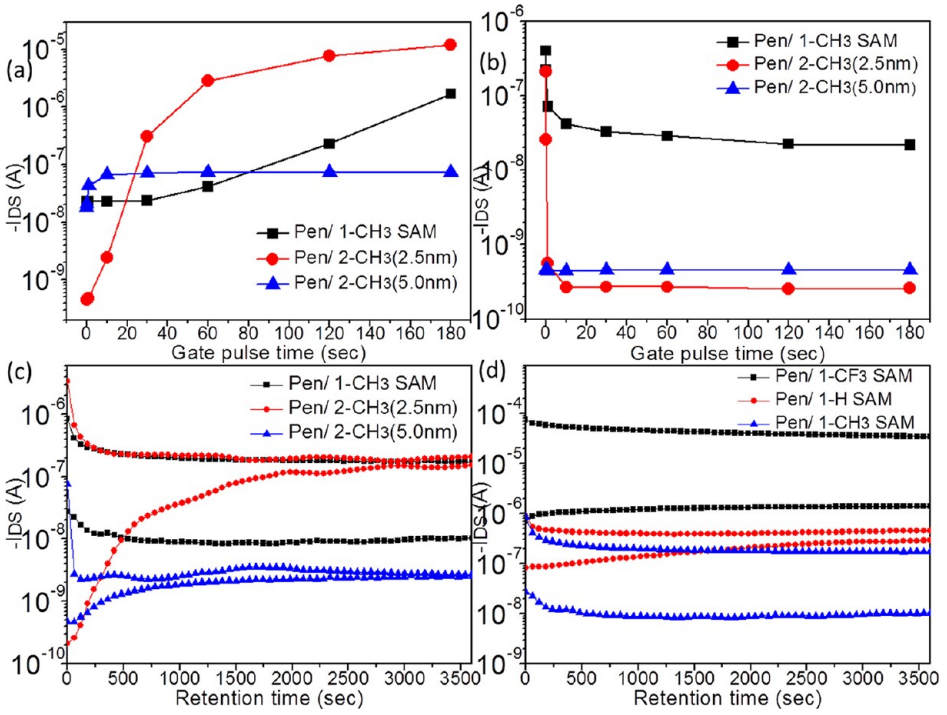

Figure 11. (a, b) Source−drain current as a function of gate pulse time for the device of **1-CH$_3$** monolayer and device **2-CH$_3$** with a nominal thickness of 2.5 nm and 5.0 nm, respectively. (c, d) Retention characteristics of the corresponding devices with monolayer of **1-CF$_3$**, **1-H** and **1-CH$_3$**, respectively.

devices with 2.5 nm of **2-CH$_3$** at the interface, the equivalent amount of one monolayer but in the form of multilayered clusters, the hysteresis is much larger than that in the case of **1-CH$_3$** SAM. This can be rationalized on the basis of the proximity of conducting channel and the trap sites, which leads to more efficient charge transfer to the azobenzene moieties, when the multilayer azobenzene clusters are surrounded and embedded in the pentacene film. A substituent effect is also observed when the V_g sweep range increases progressively for **2-CH$_3$** system, say, from +20 V to −20 V and then +40 to −40 V, +60 V to −60 V and etc., the threshold voltage shifts in the negative direction increased faster than in the positive direction (Figure 10b). This suggests that holes are trapped more efficiently than the electrons. Whereas for **2-CF$_3$** system, the same increase in V_g sweep range results in threshold voltage shifting in the positive direction faster than in the negative direction (Figure 10c), meaning the **2-CF$_3$** system trapped electrons more efficiently than holes.

Figure 11 shows the I_{DS} as a function of gate pulse duration for the **1-CH$_3$** monolayer system and **2-CH$_3$** cluster system at two thicknesses. For the **1-CH$_3$** monolayer system, I_{DS} increased gradually and did not reach the maximum after 180 s of +100 V pulse (Figure 11a), indicating that these azobenzene moieties were charged negatively rather slowly. On the other hand, the **2-CH$_3$** system reached its maximum current much faster, presumably because the charging of the azobenzenes in these clusters are faster because of the facile transfer of charges between pentacene and the azobenzene moieties. For −100 V pulse, the current in the system comprising **1-CH$_3$** monolayer gradually decreases to its minimum, whereas the **2-CH$_3$** cluster system shows a very rapid current decay, presumably due to a much faster charging of the clusters with holes because of a good proximity of pentacene molecules to the azobenzene moieties in the clustered form. However, virtually for the same reason, the retention time of these systems has an opposite trend: the monolayer **1-CH$_3$** system has a much longer retention time than the clustered **2-CH$_3$** system as the trapped charges are retained more effectively in a monolayer. Thus the on/off ratio remain nearly unchanged after 1 h for **1-CH$_3$** system but decreased to ∼1 after 50 min for 2.5 nm **2-CH$_3$** system and even quicker for 5 nm **2-CH$_3$** system (Figure 11c). A comparison of differently substituted monolayers, the retention characteristics are good for both **1-CH$_3$** and **1-CF$_3$** systems but slightly faster decay for the **1-H** system was observed.

CONCLUSION

In conclusion, we demonstrated in this work that azobenzene moieties can be effective trapping sites to reach electric bistability in a pentacene-based transistors. The trapping sites can be introduced either in an oriented single silane monolayer film or discrete clusters of multilayers of azobenzene acids at the dielectric/pentacene interface. The charge carriers can be trapped into these sites either photochemically or by electric gate biasing. Photo irradiation results in excitation of azobenzene moieties, followed by charge transfer between pentacene and the azo dyes. Either electron or hole charges can be transferred depending on the substituent on the azobenzene moiety, leading to threshold voltage shifts in different directions when transfer curves are measured. Electric bias can also lead to trapping of carriers on the azobenzene sites at the interface, with efficiency of charge trapping depending on the ability of the substituent on the azobenzene to stabilize the specific charges, as well as the accessibility of the trapping sites to the charge carriers in pentacene film. Electric bistability, and the response time, retention characteristics, and threshold voltage shifts can be rationalized systematically. In particular, the charging of monolayer of azobenzene at the dielectric layer

surface is slower, yet the charges are well-retained. The charging of clusters embedded in the pentacene film is faster (response faster) but detrap of charges is also faster. These contrasting characteristics will be the issue to be addressed in the further design of efficient and stable organic memory devices.

■ ASSOCIATED CONTENT

Ⓢ Supporting Information

The characterization for the monolayer formation process and the synthetic procedures and characterization data for compounds **1** and **2**. This material is available free of charge via the Internet at http://pubs.acs.org.

■ AUTHOR INFORMATION

Corresponding Author

*E-mail: ytt@chem.sinica.edu.tw.

Notes

The authors declare no competing financial interest.

■ ACKNOWLEDGMENTS

The authors thank the National Science Council of Taiwan, the Republic of China, and Academia Sinica for financial support of this work.

■ REFERENCES

(1) Dimitrakopoulos, C. D.; Malenfant, P. R. L. *Adv. Mater.* **2002**, *14*, 99.
(2) Arias, A. C.; MacKenzie, J. D.; McCulloch, I.; Rivnay, J.; Salleo, A. *Chem. Rev.* **2010**, *110*, 3.
(3) Sokolov, A. N.; Tee, B. C. K.; Bettinger, C. J.; Tok, J. B. H.; Bao, Z. *Acc. Chem. Res.* **2012**, *45*, 361.
(4) Scott, J. C.; Bozano, L. D. *Adv. Mater.* **2007**, *19*, 1452.
(5) Yao, J.; Zhong, L.; Zhang, Z.; He, T.; Jin, Z.; Wheeler, P. J.; Natelson, D.; Tour, J. M. *Small* **2009**, *5*, 2910.
(6) Huang, Y. L.; Lu, Y.; Niu, T. C.; Huang, H.; Kera, S.; Ueno, N.; Wee, A. T. S.; Chen, W. *Small* **2012**, *8*, 1423.
(7) Cho, B.; Song, S.; Ji, Y.; Kim, T. W.; Lee, T. *Adv. Funct. Mater.* **2011**, *21*, 2806.
(8) Guo, Y.; Yu, G.; Liu, Y. *Adv. Mater.* **2010**, *22*, 4427.
(9) Naber, R. C. G.; Asadi, K.; Blom, P. W. M.; de Leeuw, D. M.; de Boer, B. *Adv. Mater.* **2010**, *22*, 933.
(10) Zhang, H.; Guo, X.; Hui, J.; Hu, S.; Xu, W.; Zhu, D. *Nano Lett.* **2011**, *11*, 4939.
(11) Khan, M. A.; Bhansali, U. S.; Alshareef, H. N. *Adv. Mater.* **2012**, *24*, 2165.
(12) Leong, W. L.; Mathews, N.; Tan, B.; Vaidyanathan, S.; Dötz, F.; Mhaisalkar, S. *J. Mater. Chem.* **2011**, *21*, 5203.
(13) Baeg, K. J.; Khim, D.; Kim, J.; Yang, B. D.; Kang, M.; Jung, S. W.; You, I. K.; Kim, D. Y.; Noh, Y. Y. *Adv. Funct. Mater.* **2012**, DOI: 10.1002/adfm.201200290.
(14) Tseng, C. W.; Chen, Y. L.; Tao, Y. T. *Org. Electron.* **2012**, *13*, 1436.
(15) Zhou, Y.; Han, S. T.; Xu, Z. X.; Roy, V. A. L. *Adv. Mater.* **2012**, *24*, 1247.
(16) Chen, C. M.; Liu, C. M.; Wei, K. H.; Jeng, U. S.; Su, C. H. *J. Mater. Chem.* **2012**, *22*, 454.
(17) Tseng, C. W.; Tao, Y. T. *ACS Appl. Mater. Interfaces* **2010**, *2*, 3231.
(18) Heremans, P.; Gelinck, G. H.; Müller, R.; Baeg, K. J.; Kim, D. Y.; Noh, Y. Y. *Chem. Mater.* **2011**, *23*, 341.
(19) Li, C.; Ly, J.; Lei, B.; Fan, W.; Zhang, D.; Han, J.; Meyyappan, M.; Thompson, M.; Zhou, C. *J. Phys. Chem. B* **2004**, *108*, 9646.
(20) Wu, W.; Zhang, H.; Wang, Y.; Ye, S.; Guo, Y.; Di, C.; Yu, G.; Zhu, D.; Liu, Y. *Adv. Funct. Mater.* **2008**, *18*, 2593.
(21) Russew, M. M.; Hecht, S. *Adv. Mater.* **2010**, *22*, 3348.
(22) Jung, U.; Filinova, O.; Kuhn, S.; Zargarani, D.; Bornholdt, C.; Herges, R.; Magnussen, O. *Langmuir* **2010**, *26*, 13913.
(23) Crivillers, N.; Orgiu, E.; Reinders, F.; Mayor, M.; Samorì, P. *Adv. Mater.* **2011**, *23*, 1447.
(24) Kobayashi, S.; Nishikawa, T.; Takenobu, T.; Mori, S.; Shimoda, T.; Mitani, T.; Shimotani, H.; Yoshimoto, N.; Ogawa, S.; Iwasa, Y. *Nat. Mater.* **2004**, *3*, 317.
(25) Islam, M. M.; Pola, S.; Tao, Y. T. *ACS Appl. Mater. & Interf.* **2011**, *3*, 2136.
(26) Lim, S. L.; Li, N. J.; Lu, J. M.; Ling, Q. D.; Zhu, C. X.; Kang, E. T.; Neoh, K. G. *ACS Appl. Mater. & Interf.* **2009**, *1*, 60.
(27) Kim, M.; Safron, N. S.; Huang, C.; Arnold, M. S.; Gopalan, P. *Nano Lett.* **2012**, *12*, 182.
(28) Zhang, H.; Guo, X.; Hui, J.; Hu, S.; Xu, W.; Zhu, D. *Nano Lett.* **2011**, *11*, 4939.
(29) Orgiu, E.; Crivillers, N.; Herder, M.; Grubert, L.; Patzel, M.; Frisch, J.; Pavlica, E.; Duong, D. T.; Bratina, G.; Salleo, A.; Koch, N.; Hecht, S.; Samori, P. *Nat. Chem.* **2012**, *4*, 675.
(30) Liu, Z. F.; Hashimoto, K.; Fujishima, A. *Nature* **1990**, *347*, 658.
(31) Howarter, J. A.; Youngblood, J. P. *Langmuir* **2006**, *22*, 11142.
(32) Wang, S. Y.; Huang, D. C.; Tao, Y. T. *J. Chin. Chem. Soc.* **2012**, *59*, 9.
(33) Wang, C.; Dong, H.; Hu, W.; Liu, Y.; Zhu, D. *Chem. Rev.* **2012**, *112*, 2208.
(34) Steudel, S; De Vusser, S.; De Jonge, S.; Janssen, D.; Verlaak, S.; Genoe, J.; Heremans, P. *Appl. Phys. Lett.* **2004**, *85*, 4400.
(35) Lee, H. S.; Kim, D. H.; Cho, J. H.; Hwang, M.; Jang, Y.; Cho, K. *J. Am. Chem. Soc.* **2008**, *130*, 10556.
(36) Ikegami, A.; Suda, M.; Watanabe, T.; Einaga, Y. *Angew. Chem., Int. Ed.* **2009**, *48*, 1.
(37) Maliakal, A.; Raghavachari, K.; Katz, H.; Chandross, E.; Siegrist, T. *Chem. Mater.* **2004**, *16*, 4980.
(38) Evans, S. D.; Johnson, S. R.; Ringsdorf, H.; Williams, L. M.; Wolf, H. *Langmuir* **1998**, *14*, 6436.
(39) Tamada, K.; Akiyama, H.; Wei, T. X.; Kim, S. A. *Langmuir* **2003**, *19*, 2306.
(40) Baeg, K. J.; Noh, Y. Y.; Sirringhaus, H.; Kim, D. Y. *Adv. Funct. Mater.* **2010**, *20*, 224.
(41) Dong, H.; Zhu, H.; Meng, Q.; Gong, X.; Hu, W. *Chem. Soc. Rev.* **2012**, *41*, 1754.
(42) Podzorov, V.; Gershenson, M. E. *Phys. Rev. Lett.* **2005**, *95*, 016602.
(43) Guo, Y.; Di, C. A.; Ye, S.; Sun, X.; Zheng, J.; Wen, Y.; Wu, W.; Yu, G.; Liu, Y. *Adv. Mater.* **2009**, *21*, 1.